



Dyskinesia is Closely Associated with Synchronization of Theta Oscillatory Activity Between the Substantia Nigra Pars Reticulata and Motor Cortex in the Off L-dopa State in Rats

Jiazhi Chen¹ · Qiang Wang^{1,3} · Nanxiang Li¹ · Shujie Huang¹ · Min Li¹ · Junbin Cai¹ · Yuzheng Wang² · Huantao Wen¹ · Siyuan Lv¹ · Ning Wang² · Jinyan Wang² · Fei Luo² · Wangming Zhang¹

Received: 6 March 2020 / Accepted: 13 May 2020 / Published online: 19 November 2020
© Shanghai Institutes for Biological Sciences, CAS 2020

Abstract Excessive theta (θ) frequency oscillation and synchronization in the basal ganglia (BG) has been reported in elderly parkinsonian patients and animal models of levodopa (L-dopa)-induced dyskinesia (LID), particularly the θ oscillation recorded during periods when L-dopa is withdrawn (the off L-dopa state). To gain insight into processes underlying this activity, we explored the relationship between primary motor cortex (M1) oscillatory activity and BG output in LID. We recorded local field potentials in the substantia nigra pars reticulata (SNr) and M1 of awake, inattentive resting rats before and after L-dopa priming in Sham control, Parkinson disease model, and LID model groups. We found that chronic L-dopa increased θ synchronization and information flow between the SNr and M1 in off L-dopa state LID rats, with a SNr-to-M1 flow directionality. Compared with the on state, θ oscillational activity (θ synchronization and information

flow) during the off state were more closely associated with abnormal involuntary movements. Our findings indicate that θ oscillation in M1 may be consequent to abnormal synchronous discharges in the BG and support the notion that M1 θ oscillation may participate in the induction of dyskinesia.

Keywords Parkinson's disease · Dyskinesia · Substantia nigra pars reticulata · Primary motor cortex · Synchronization

Introduction

Commonly, Parkinson's disease (PD) patients who are treated chronically with L-dopa experience a disabling motor complication known as levodopa (L-dopa)-induced dyskinesia (LID) [1, 2]. The main pathophysiological mechanisms proposed to underlie LID are maladaptive synaptic remodeling [3], activation of the D1-direct pathway of the basal ganglia (BG), and distorted BG output from the substantia nigra pars reticulata (SNr)/internal globus pallidus (GPi) [4–6].

Acute administration of L-dopa significantly increases the power of θ oscillation (2 Hz–10 Hz) in elderly PD patients during the on state with [7, 8] or without dyskinesia [9–11]. These findings indicate that θ oscillation may mediate motor restoration or have pro-kinetic effects in PD patients [7, 12–14]. Importantly, θ oscillations in the range of 2 Hz–7 Hz have been recorded in the subthalamic nucleus (STN) during the off L-dopa dyskinesia state in a group of PD patients with a mean disease history of 14.1 years [13]. However, the lack of electrophysiological data from the BG of early PD patients has resulted in a poor

Jiazhi Chen and Qiang Wang contributed equally to this work.

✉ Fei Luo
luof@psych.ac.cn

✉ Wangming Zhang
wzhang@vip.126.com

¹ The National Key Clinic Specialty, The Engineering Technology Research Center of the Ministry of Education of China, Guangdong Provincial Key Laboratory on Brain Function Repair and Regeneration, Department of Neurosurgery, Zhujiang Hospital, Southern Medical University, Guangzhou 510282, China

² Key Laboratory of Mental Health, Institute of Psychology, Chinese Academy of Sciences, Beijing 100101, China

³ Movement Disorders and Neuromodulation Unit, Department for Neurology, Charité - University Medicine Berlin, 10117 Berlin, Germany

understanding of the cumulative effects of long-term L-dopa administration.

Enhanced θ oscillations (4 Hz–8 Hz) recorded in the dorsolateral striatum (dStr) of off-state LID model rats have been associated with chronic synaptic plasticity in the striatum [15]. Such off-state θ oscillation appears to result from repeated dopamine (DA) stimulation and plasticity within the BG [16]. Although θ oscillation in the off L-dopa state dyskinesia may share mechanisms with that in on-state dyskinesia, it is unclear how θ oscillation works in the BG during L-dopa off-state dyskinesia.

The effectiveness of deep brain stimulation of the GPi in LID patients with dyskinesia [17, 18] and of the entopeduncular nucleus in LID model rats [15] have highlighted the importance of firing rate or pattern within BG output structures in the modulation of electrophysiological changes in BG output [17, 19]. However, the effects of regulation of BG output nuclei on downstream structures, including the motor cortex (M1), are not known.

There has been a growing interest in the electrophysiology of M1 during dyskinesia [14, 20–23]. Animal models of LID provide an opportunity to investigate the emergence of a synchronization of activity between M1 and BG output structures. Strong M1-SNr beta (β) synchronization in PD models can be suppressed by L-dopa [24], raising the possibility that abnormal M1-SNr synchronization may also exist in LID due to chronic L-dopa priming. Moreover, oscillatory activity in the SNr indirectly reflects the comprehensive synchronous activity of the BG network [25]. Such findings led us to investigate oscillatory activity in the SNr and M1 after prolonged L-dopa treatment in PD.

The serotonergic system has been implicated in LID induction [26–28] owing to serotonergic neurons containing the molecular machinery to convert L-dopa into DA. Consequently, when nigrostriatal DA terminals have largely degenerated and the remaining DA neurons are in an injured state [29], dopaminergic neuron-derived DA can be supplemented by serotonergic neuron-derived DA [26, 30]. However, because this DA release from serotonergic terminals lacks a negative feedback regulation mechanism, it can stimulate postsynaptic DA receptors in an uncontrolled manner [26, 31], thereby producing dyskinesia.

The mixed type 1A/1B serotonergic receptor agonist eltoprazine (Elto) has been shown to reduce signs of dyskinesia in LID rats [27, 32] and PD patients [33, 34]. In a recent study, we showed that chronic Elto reduces the severity of abnormal involuntary movements (AIMs) and that this effect is associated with a reduced θ oscillation flow in the direct pathway of the BG [35]. Regarding the mechanism of Elto's dyskinesia-alleviating effect, chronic Elto has been reported to normalize phosphorylated ERK levels in the striatum and reduce the sensitization of

GABAergic spiny neurons (in the direct pathway) to L-dopa, the over-activation of which has been correlated with dyskinesias [9, 27].

In the present study, we aimed to investigate the relationship between L-dopa induced dyskinesia and synchronous activity of the SNr-M1 circuit in off L-dopa state LID rats. Therefore, we simultaneously recorded LFPs from the M1 and SNr in Sham, PD and LID rats (PD rats with L-dopa-induced dyskinesias after chronic L-dopa treatment). Furthermore, The type 1A/1B serotonin receptor agonist Elto, type D1/D5 DA receptor agonist SKF 38393, and type D2/D3 DA receptor agonist quinpirole were used to probe the correlation between θ oscillational activities activity and dyskinesia.

Materials and Methods

All experimental procedures were performed in accordance with the National Institutes of Health guide for the care and use of Laboratory animals (NIH Publications No. 8023, revised 1978) and approved by the Institutional Animal Ethics Committee of Southern Medical University of China. Appropriate measures were taken to minimize the animals' pain and discomfort.

Animals

Sprague-Dawley rats were housed under a 12 h:12 h reversed light cycle (lights on at 07:00 am) with *ad libitum* access to water. Daily food intake was limited to ~16 g for weight maintenance. For the week before the experiment, rats were each handled for ~6 min each day.

A total of 39 rats were used, including 31/39 that received a 6-hydroxydopamine (6-OHDA) injection into the right medial forebrain bundle (MFB) to induce a unilateral PD model. The remaining 8 rats each received an intra-MFB injection with 0.02% ascorbate saline solution (vehicle) and thus constituted a Sham group. 25/31 rats were regarded as PD model rats after apomorphine (APO) challenge (modeling success rate, 80%). 13/25 PD model rats were treated with intraperitoneal injection (*i.p.*) 6 mg/kg L-dopa plus 12 mg/kg *i.p.* benserazide hydrochloride (both from Sigma) to induce dyskinesia (LID group) or injected with Saline (Fig. 1A, B). The main experimental treatment groups were as follows: Sham group ($n = 8$), PD group ($n = 12$), and LID group ($n = 13$). All 39 rats were implanted with microelectrodes.

Experimental Procedures

Based on our histological results, 2/12, 2/13, and 1/8 rats were eliminated from the PD, LID, and Sham groups,

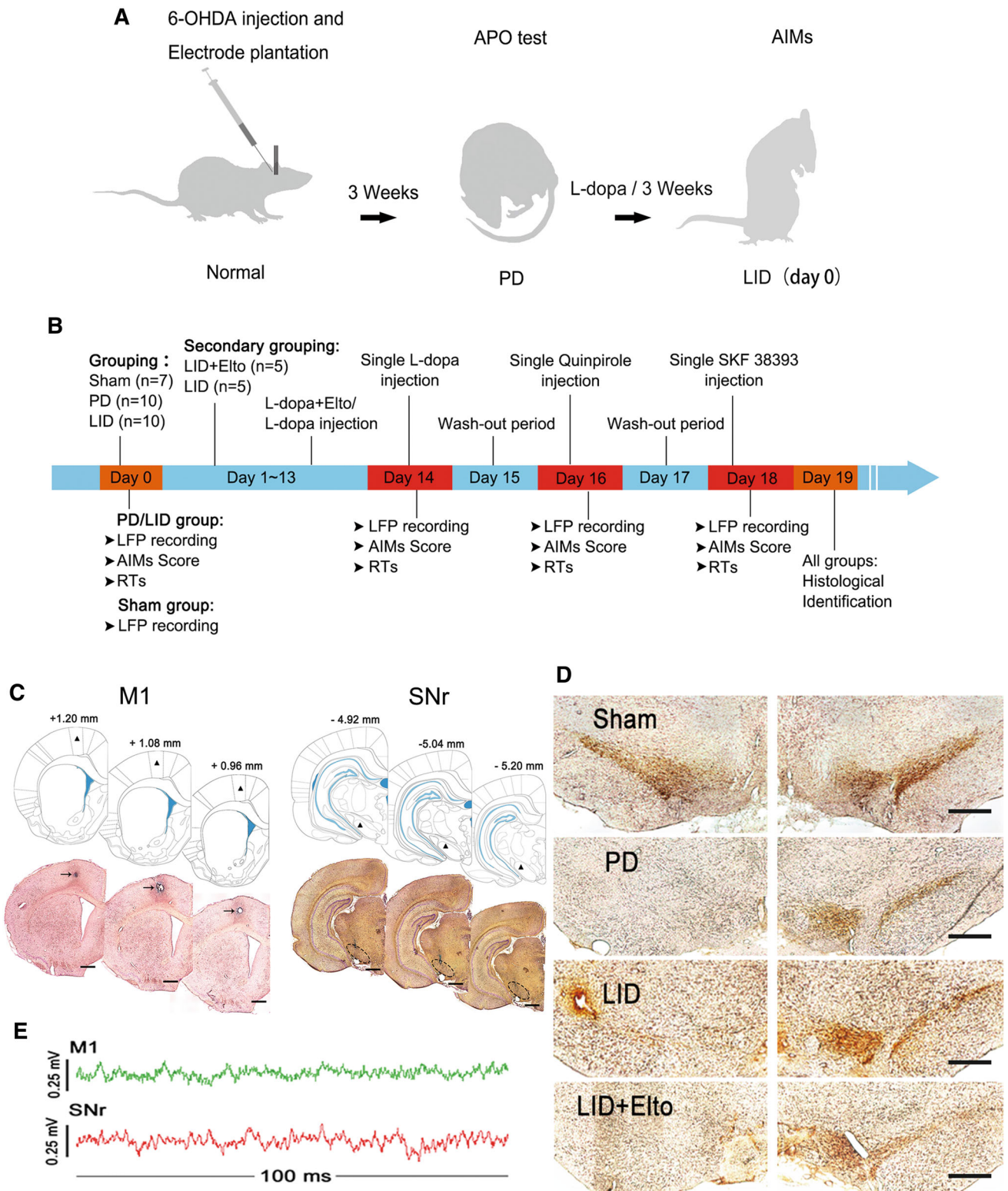


Fig. 1 Experimental procedures and histology. **A** Schematic of PD and LID model generation. **B** Overview of the experimental design. **C** Electrode implantation sites. Targets (black triangles) are shown above in brain map images (see Methods for coordinates). Representative Nissl stained sections showing accurately located electrode tips

targeting M1 layers 5/6 (left, black arrows) and SNr (right, dotted line-enclosed areas). Scale bars, 1 mm. **D** Representative TH immunolabeling of DA neurons in the SNc by (sub)group. **E** LFP raw data samples for M1 (green) and the SNr (red); A 100-ms time series is shown (calibration: horizontal 100 ms; vertical, 250 μ V).

respectively, for misplaced electrode tips. In addition, one rat's electrode fell off consequent to AIMs after acute L-dopa administration in the LID group. Thus, the final group numbers were as follows: PD, $n = 10$; LID, $n = 10$; and Sham, $n = 7$. After LID/PD modeling (Fig. 1A), on day 0, local field potentials (LFPs) were recorded before (off state) and after (on state) a single priming injection of L-dopa (6 mg/kg, *i.p.*) and benserazide hydrochloride (12 mg/kg, *i.p.*). PSD, coherence, and Granger causality data were collected for LFP analysis. Pearson correlation analysis was used to evaluate the relationship between oscillatory activity and AIM scores. To further examine the θ functional connectivity between the SNr and M1 in off-state LID rats, they were divided into two subgroups: LID and LID+Elto ($n = 5$ each). Rats were subjected to chronic Elto (8 mg/kg, *i.p.*) and L-dopa (6 mg/kg, *i.p.*) for 13 days with L-dopa (6 mg/kg, *i.p.*) priming (Fig. 1B). The Elto dosage regimen was based on a previous study [32]. On day 14, a single L-dopa (6 mg/kg, *i.p.*) plus benserazide hydrochloride (12 mg/kg, *i.p.*) injection was used to acutely induce AIMs. After a 24-h washout period, on day 16, quinpirole (0.2 mg/kg, *i.p.*) was used to induce AIMs in the LID and LID+Elto subgroups (Fig. 1B). After another 24-h washout period, on day 18, the type D1/D5 DA receptor agonist SKF 38393 (1.0 mg/kg, *i.p.*) was used to induce AIMs. These doses of quinpirole [22] and SKF 38393 [36] have been shown to induce AIMs in 6-OHDA-lesioned rats. LFP recording and analyses were performed on days 14, 16, and 18, before the drug challenges. During the drug challenges, AIM data - including reaction time (RT), AIM subtype scores for axial, limb, and orolingual AIMs, and total AIM score - were recorded on days 14, 16, and 18 (Fig. 1B).

Unilateral Intra-MFB 6-OHDA Injection and Electrode Implantation

After anesthesia with sodium pentobarbital (50 mg/kg, *i.p.*), each rat's head was fixed in a stereotaxic apparatus with the tooth bar set to -3.3 mm. Each rat received preoperative penicillin (16,000 U, intramuscular) to prevent infection. The skull was exposed and two holes were bored above the right MFB. 4 μ L of 6-OHDA (3 μ g/ μ L, Sigma) dissolved in 0.2 mg/mL L-ascorbic acid in 0.9% w/v saline was injected (1 μ L/min) into the right MFB at the following coordinates (in mm relative to bregma): -1.8 antero-posterior (AP); 2.0 medio-lateral (ML); and -8.2 dorsal-ventral (DV; below the skull surface) (Paxinos and Watson, 2007). Rats received desipramine (noradrenergic reuptake inhibitor; 15 mg/kg, *i.p.*; Sigma) 25 min before the 6-OHDA injection to minimize damage to noradrenergic neurons. Sham rats received a 4 μ L injection of ascorbic saline into the right MFB. Electrode bundles consisted of 8 stainless steel Teflon-

insulated microwires (50 μ m diameter, arranged in a $3 \times 3 \times 2$ configuration, 250 μ m spacing between microwires; Plexon, Hong Kong) were implanted vertically in the right M1 layers V/VI ($+1.08$ mm AP, $+2.3$ mm ML, and -2.0 mm DV) and the SNr (-5.04 mm AP, $+2.5$ mm ML, and -8.0 mm DV). The microelectrode arrays were secured to the cranium with stainless steel jeweler's screws and dental cement. A screw placed above the cerebellum served as a ground; it was placed in contact with the dura, and ground wires were wrapped around it.

Two weeks after the operation, unilateral DA depletion was assessed by a challenge with APO (0.25 mg/kg, *i.p.*; Sigma). Rotations were counted, starting 5 min after the APO injection. DA depletion was considered sufficient if a rat rotated toward the non-lesioned side ≥ 80 times more than it rotated toward the lesioned side in a 20-min period. DA-depleted rats in the LID group received L-dopa (6 mg/kg, *i.p.*; Sigma) plus benserazide (12 mg/kg, *i.p.*; Sigma) for 21 days to induce dyskinesia [37].

AIM Scores

L-dopa-induced AIMs were scored according to a rat dyskinesia scale [22, 38]. The severity of dyskinesia was evaluated on an AIM scale [23, 39]; axial, forelimb, and orolingual dyskinesias were each scored from 0 to 4: 0, absence of abnormal movements; 1, dyskinesia occurred $<50\%$ of the observational period; 2, dyskinesia occurred $>50\%$ of the observational period; 3, constant dyskinesia that could be interrupted artificially; 4, constant dyskinesia that could not be interrupted. After L-dopa injection, rats were video-recorded and observed for 180 min; AIMs were evaluated for 60 s within each 20-min interval (nine intervals, maximum AIM value, 108).

RT of AIMs

The time interval between the dopaminergic drug injections and the emergence of AIMs is considered to be the RT of AIMs, as described previously [35].

In vivo Electrophysiology

LFPs were recorded extracellularly in the SNr and M1 with a 128-channel data acquisition system (Cerebus, Blackrock Microsystems Inc., Salt Lake City, UT, USA) before and 60 min after L-dopa injection. LFPs were recorded with miniature wireless head-stages (W16 system, Triangle BioSystems International, Harvard Bioscience Inc., Durham, NC, USA) [40]. LFPs were recorded in five 2-min sessions (total epoch, 10 min) while videos were recorded simultaneously. LFP oscillations were recorded at a sampling frequency of 10 KHz, amplified (300 \times), and

band pass-filtered (0.3 Hz–500 Hz); 50-Hz signals were removed from the digitized signals to prevent inclusion of the power line interface.

Histology

Rats were anesthetized with an overdose of pentobarbital, and then a +20- μ A current was passed through the recording electrodes for 30 s to deposit iron ions. The rats were perfused transcardially with 300 mL saline (0.9% w/v), followed by 400 mL of ice-cold paraformaldehyde and potassium ferricyanide solution (4% and 5% w/v in 0.1 mol/L phosphate-buffered saline, respectively). The brains were immersed in 4% paraformaldehyde for 12 h and then dehydrated in sucrose solution (25% w/v in 0.1 mol/L phosphate-buffered saline) until they sank completely. Coronal 30- μ m sections containing the substantia nigra compacta (SNc) and the M1/SNr were cut on a Leica cryostat (Leica CM1900, Germany). M1 was examined in the coronal plane from target-adjacent brain atlas plates +1.20 AP to +0.96 AP (encompassing the target at 1.08 AP), whereas the SNr was examined in the coronal plane from target-adjacent brain atlas plates –4.92 AP to –5.04 AP (encompassing the target at –5.04 AP). M1 and SNr-containing sections were Nissl stained to facilitate confirmation of electrode tip locations; only rats with accurate electrode placements terminating in the M1 and SNr were included in the statistical analyses. Tyrosine hydroxylase was immunolabeled in SNc-containing sections as described in our previous report [41].

Data Analysis

LFP recordings were obtained during 10-min epochs during an inattentive rest state before and after an L-dopa challenge. PSD, coherence, and Granger causality were assessed over the θ (4 Hz–10 Hz) and high β (20 Hz–38 Hz) frequency ranges in representative 120-s sessions within the 10-min epoch in M1 and the SNr. For each rat in each behavioral state, LFP data from two wires per epoch were used for further analyses.

Spectral Analysis and Coherence of LFPs

We used multi-taper spectral estimation to calculate PSDs using the MatLab toolbox Chronux (<http://chronux.org>) [42]. During the recording in the resting and AIMs states, 120-s epochs free of major artifacts were selected for further calculation (PSD, coherence, and Granger causality). LFP recordings were sampled at 1 kHz (frequency resolution, 1 Hz); each 120-s period was segmented into 120 1-s bins. The 50-Hz frequency was removed. The following calculation parameters were applied: params. fpass = [0,

50] (target frequency range, 0 Hz–50 Hz) and params. tapers = [3, 5] (best degree of spectral smoothing at time-bandwidth product of 3 and 5 tapers) [35, 43]. To assess functional relationships between M1 and the SNr before and after a resting-state L-dopa challenge, coherence was determined by measuring the linear correlation between two digitized signals across frequencies, with values ranging from 0 (no linear association) to 1 (perfect linear association). Coherences (\sim 1 Hz resolution) were calculated with the following Chronux parameters: params. fpass = [0, 50] and params. tapers = [7, 13] (<http://chronux.org>). Low values of coherence between brain regions indicate an unsynchronized signal and high values indicate a high degree of synchronization [44].

Granger Causal Analysis

Partial Granger causal analysis in the target frequency bands (θ , 4 Hz–10 Hz; and high β , 20 Hz–38 Hz) was assessed between M1 and the SNr based on multivariate autoregressive modeling, with two jointly-distributed variables (time series X and Y). According to Granger causality, if prior Y values are predictive of future X values, then Y is said to have a causal influence on X and Y \rightarrow X information flow is affirmed, enabling the directionality of functional connections between brain areas to be assessed [45]. Therefore, Granger causality gives insight into the causal interactions between brain areas. To begin with, model order was estimated, and the best model order was chosen by Akaike Information Criterion, and Vector Autoregressive (VAR) model estimation using the targeted model order was conducted through the Levinson, Wiggins and Robinson algorithm. Further, the autocovariance sequence was calculated according to the VAR model. Finally, partial granger causality in the frequency domain was calculated using the autocovariance sequence [46].

Statistics

All data are reported as means with standard errors (SEMs). Sham, PD, and LID group data were subjected to analyses of variance (ANOVAs) and repeated measures (rm) ANOVAs. If significant rmANOVA results were obtained, Bonferroni's post hoc tests were applied. Total AIMs/PSD/coherence/Granger causality between the LID and LID+Elto LID subgroups were compared by Student's t tests. Correlations between θ coherence/Granger causality and AIMs were calculated by Pearson correlation analysis. P values < 0.05 were considered statistically significant. The analyses were conducted in Prism 5.0 software by Graphpad [27].

Results

M1 and SNr oscillations after DA Denervation and Chronic L-dopa Priming

Off L-dopa State PSD

Off L-dopa state LFP recordings on day 0 served as baseline data. For θ oscillations in M1, ANOVA showed main effects of L-dopa state ($F_{1,24} = 3.430$, $P > 0.05$) and group ($F_{2,24} = 55.171$, $P < 0.001$) as well as a significant L-dopa state (2) \times group (3) interaction ($F_{2,24} = 6.688$, $P < 0.05$). We found that θ oscillation in M1 was significantly higher in the LID group than that in PD group during the off L-dopa state (Fig. 2C; Bonferroni's *post-hoc*, $P = 0.002$); M1 θ band power in the Sham group was similar to that in the PD group (Bonferroni's *post-hoc*, $P = 1.000$).

Likewise, θ oscillation in the SNr was significantly higher in the LID group than in the PD group during the off state (Fig. 2D; rmANOVA group effect, $F_{2,24} = 10.073$,

$P < 0.01$; and L-dopa (2) \times group (3) interaction, $F_{2,24} = 10.805$, $P < 0.001$; Bonferroni's *post-hoc* test, $P = 0.042$). The θ band power in the SNr for the Sham group was similar to that for the PD group (Fig. 2D; Bonferroni's *post-hoc*, $P = 0.163$).

The high β oscillation in M1 was significantly greater in the 6-OHDA-lesioned PD group than in the Sham group (Fig. 2C; rmANOVA, L-dopa state (2) \times group (3) ($F_{2,24} = 3.715$, $P < 0.05$; Group: $F_{2,24} = 26.385$, $P < 0.001$; Bonferroni's *post-hoc*: $P < 0.001$). Meanwhile, the LID group was found to have significantly lower power in the β band during the off L-dopa state than was found for the PD group (Fig. 2C; Bonferroni's *post-hoc*, $P < 0.001$). The β band power in the SNr was similar in these two groups, indicating that 6-OHDA lesioning did not alter the β band power in the SNr (ANOVA: non-significant L-dopa state effect $F_{1,24} = 1.114$, group effect $F_{2,24} = 2.907$, and L-dopa state (2) \times group (3) interaction $F_{2,24} = 0.443$, all $P > 0.05$; Fig. 2D).

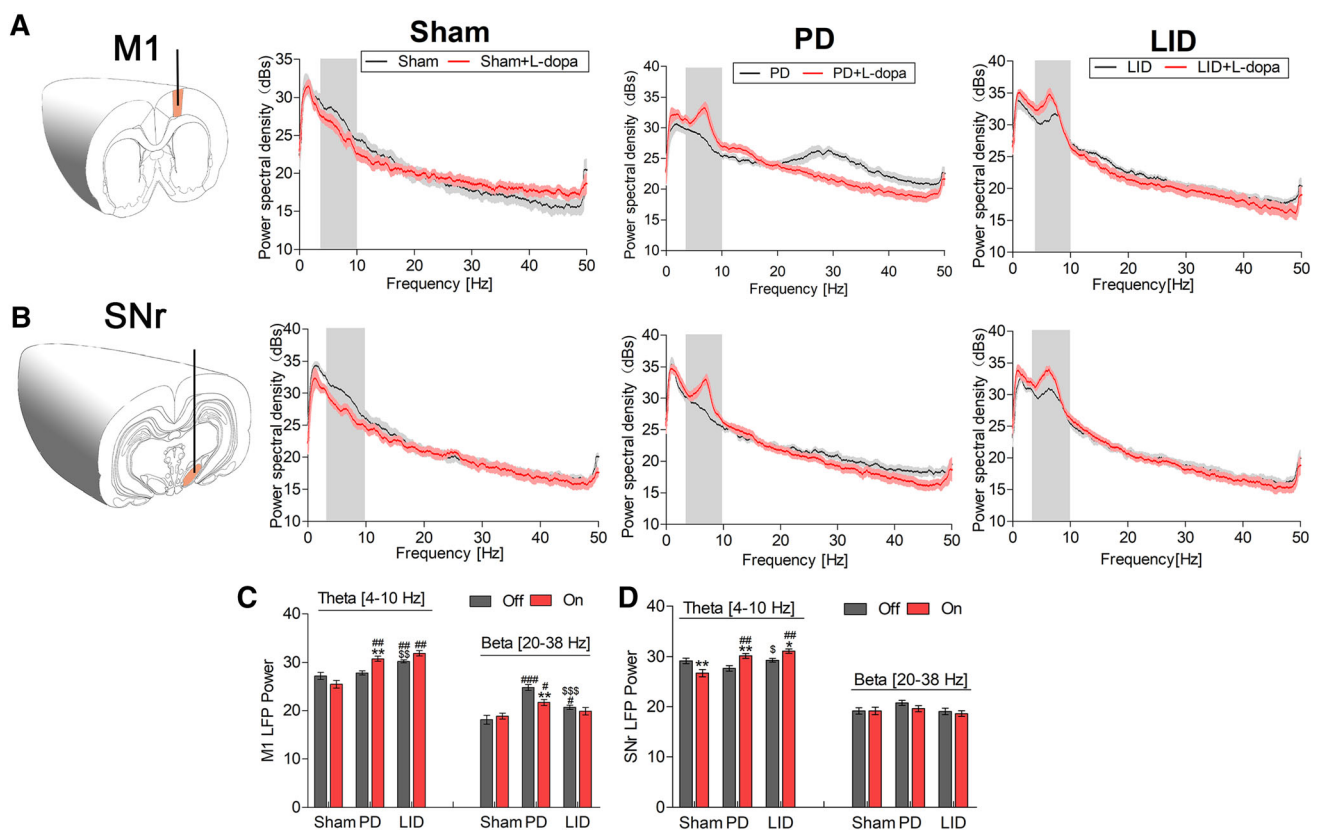


Fig. 2 PSD curves and quantification of target frequency bands. **A** Three-dimensional schematic of LFP recording sites in M1. Representative PSD spectrum plots for M1 are shown before (off-state, black) and after (on-state, red) L-dopa challenge by group: Sham ($n = 7$), PD ($n = 10$), and LID ($n = 10$). **B** Three-dimensional schematic of LFP recording sites in the SNr. Representative PSD spectrum plots for the SNr before (off-state, black) and after (on-state,

red) L-dopa challenge by group (as in panel A). **C, D** Summaries of θ - and high β -band data (mean \pm SEM) extracted for comparison within and between groups. Shaded areas in panels A and B show the θ frequency band (4 Hz–10 Hz); rmANOVA (L-dopa \times Group) followed by Bonferroni's *post-hoc* test, $*P < 0.05$, $**P < 0.01$, $***P < 0.001$ vs. off state; # markers vs. Sham; \$ markers vs. off-state PD.

On L-dopa State PSD

On-state LFPs were recorded 60 min after a single injection of 6 mg/kg L-dopa plus 12 mg/kg benserazide on day 0 (Fig. 1B), corresponding to the time of peak dyskinesia. We found that the θ power in M1 was significantly increased in the PD group after a single application of L-dopa (on L-dopa state) compared with the off state (Fig. 2C; Bonferroni's *post-hoc*, $P = 0.002$). In M1 of the LID group, the θ power exhibited a non-significant increase after a single L-dopa priming injection (Fig. 2C; Bonferroni's *post-hoc*, $P = 0.057$). There was no statistically significant difference in θ power between the PD and LID groups in the on state (Fig. 2C; Bonferroni's *post-hoc*, $P = 0.526$). Meanwhile, M1 β band power in the PD group decreased sharply after L-dopa administration (Fig. 2C; Bonferroni's *post-hoc*, $P = 0.003$).

As shown in Fig. 2D, θ power in the SNr was significantly higher during the on L-dopa state than in the off state for both the PD and LID groups (Bonferroni's *post-hoc*, $P = 0.002$ and $P = 0.017$, respectively). SNr θ band was similar in the PD and LID groups in the on L-dopa state (Fig. 2D; Bonferroni's *post-hoc*, $P = 0.588$).

Synchronization and Causal Interactions Between M1 and the SNr After DA Denervation and Chronic L-dopa Priming

Off L-dopa State Coherence

Coherence analysis to evaluate M1-SNr synchronization in different functional states showed that chronic L-dopa increased M1-SNr θ coherence during the off L-dopa dyskinetic state (rmANOVA, interaction $F_{2,24} = 14.289$, $P < 0.001$; group $F_{2,24} = 33.358$, $P < 0.001$; Bonferroni's *post-hoc*, $P < 0.001$ for LID vs. PD and LID vs. Sham; Fig. 3B). M1-SNr θ coherence during the off state did not differ significantly between the PD and Sham groups (Bonferroni's *post hoc*, $P > 0.05$, Fig. 3B). In the off state, rmANOVA analyses showed no interaction effect in high β coherence (L-dopa state (2) \times group (3), $F_{2,24} = 0.620$, $P > 0.05$).

On L-dopa State Coherence

RmANOVAs of θ coherence in the on L-dopa state showed significant main effects of state ($F_{1,24} = 16.096$, $P < 0.01$) and group ($F_{2,24} = 32.358$, $P < 0.001$), as well as a significant state \times group interaction ($F_{2,24} = 14.289$, $P < 0.001$). As shown in Fig. 3B, a single-injection L-dopa challenge increased θ coherence in the PD group (Bonferroni's *post-hoc*, $P < 0.001$) but not in the LID group (Bonferroni's *post-hoc*, $P > 0.05$) or Sham group

(Bonferroni's *post-hoc*, $P = 0.136$). During the on state, the PD and LID groups showed similar M1-SNr coherence (Bonferroni's *post-hoc*, $P > 0.009$). Moreover, there were no notable high β (20 Hz–38 Hz) coherence between or within the groups (rmANOVA: state $F_{1,24} = 4.856$, group $F_{2,24} = 0.623$, state \times group interaction $F_{2,24} = 0.005$, all $P > 0.05$).

Off L-dopa State Granger Causality

As shown in Fig. 3C and D, Granger causality analyses of LFP signals to elucidate the functional information flow between M1 and the SNr showed enhanced resting-state SNr \rightarrow M1 θ causal information flow in the LID group relative to the PD group (rmANOVA: group $F_{2,24} = 0.980$, $P > 0.05$; L-dopa state $F_{1,24} = 96.306$, $P < 0.001$; and L-dopa state \times group interaction $F_{2,24} = 45.438$, $p < 0.001$. Bonferroni's *post-hoc*, $P < 0.001$ LID vs. PD), without a significant effect on M1 \rightarrow SNr information flow (rmANOVA: group $F_{2,24} = 0.980$, $P < 0.05$; and L-dopa state \times group interaction $F_{2,24} = 1.624$, $P > 0.05$). ANOVA showed significant effects of group ($F_{2,24} = 11.393$, $P < 0.001$) and state ($F_{1,24} = 5.924$, $P < 0.05$) on SNr \rightarrow M1 high β band information flow, but no significant state \times group interaction ($F_{2,24} = 0.620$, $P > 0.05$). Meanwhile, ANOVA showed no significant effects of group ($F_{2,24} = 0.864$, $P > 0.05$) or L-dopa state ($F_{1,24} = 0.366$, $P > 0.05$) on M1 \rightarrow SNr high β band information flow, as well as no significant state \times group interaction ($F_{2,24} = 0.182$, $P > 0.05$).

On L-dopa State Granger Causality

As shown in Fig. 3C and D, after L-dopa priming, both the PD and LID groups had markedly enhanced SNr \rightarrow M1 θ causal information compared with that seen in the off state (Bonferroni's *post-hoc*: $P < 0.001$ vs. off PD; $P < 0.001$ vs. off LID). Both the PD and LID groups were found to have greater SNr \rightarrow M1 θ information flow magnitudes in the on state than the Sham group (Bonferroni's *post-hoc*: both $P < 0.001$), with no significant difference between the PD and LID SNr \rightarrow M1 θ information flow magnitudes (Bonferroni's *post-hoc*: $P = 0.422$).

AIMs and Their Associations with θ Connectivity

On day 0, AIM subtypes (axial, limb, and orolingual) and AIM RT values were recorded after L-dopa injection (Fig. 1B). As shown in Fig. 4A and B, axial, limb, and orolingual AIM scores from 0 min to 180 min (20 min/session) after L-dopa priming were higher for the LID group than for the PD group for the 20th, 40th, 60th, 80th, 100th, 120th, 140th, and 180th min observation periods

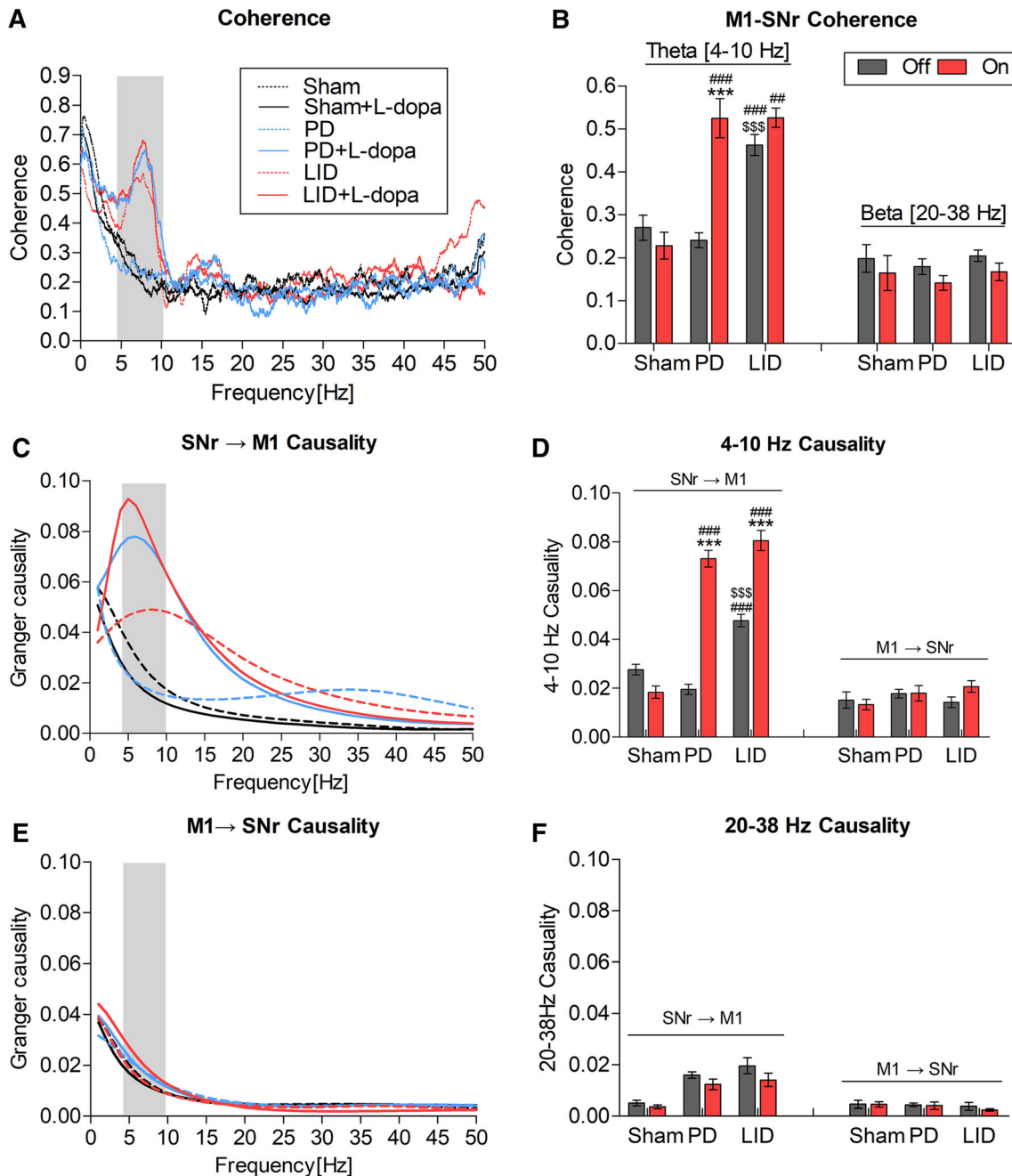


Fig. 3 M1-SNr coherence, Granger causality, and quantification of target frequency bands by group. **A** Linear graph of M1-SNr coherence within the range 0 Hz–50 Hz before (off, dotted line) and after L-dopa (on, full curve) administration for the Sham (black), PD (blue), and LID (red) groups. **B** Inter-group comparisons of mean θ and high β coherence values. **C** Linear graph showing SNr \rightarrow M1 causality before (off) and after (on) L-dopa administration (range,

0 Hz–50 Hz). **D** Inter-group comparisons of mean θ and high β band causality (SNr \rightarrow M1). **E** Linear graph showing M1 \rightarrow SNr causality before (off) and after (on) L-dopa administration (range, 0 Hz–50 Hz). **F** Inter-group comparisons of mean M1 \rightarrow SNr causality θ and β band values. All graphs show mean \pm SEM; rmANOVA (L-dopa state \times group) followed by Bonferroni's *post hoc*, * $P < 0.05$, ** $P < 0.01$, *** $P < 0.001$ (*within group; # vs. Sham; \$ vs. LID).

(Fig. 4C; rmANOVA, group effect $F_{1,18} = 388.324$, $P < 0.001$, interaction $F_{8,144} = 8.294$, $P < 0.001$; Bonferroni's *post-hoc* vs. baseline, first 6 time points $P < 0.001$, 140th min $P = 0.003$, 180th min $P = 0.005$). The total AIMs score during the on L-dopa state was greater for the LID group

(59.6 ± 0.88) than for the PD group (32.2 ± 3.39) (Fig. 4C; Student's *t* test, $P < 0.001$). Moreover, AIM RT values were shorter for the LID group (5.56 ± 0.83) than for the PD group (19.2 ± 1.62) (Fig. 4D; Student's *t* test, $P < 0.001$).

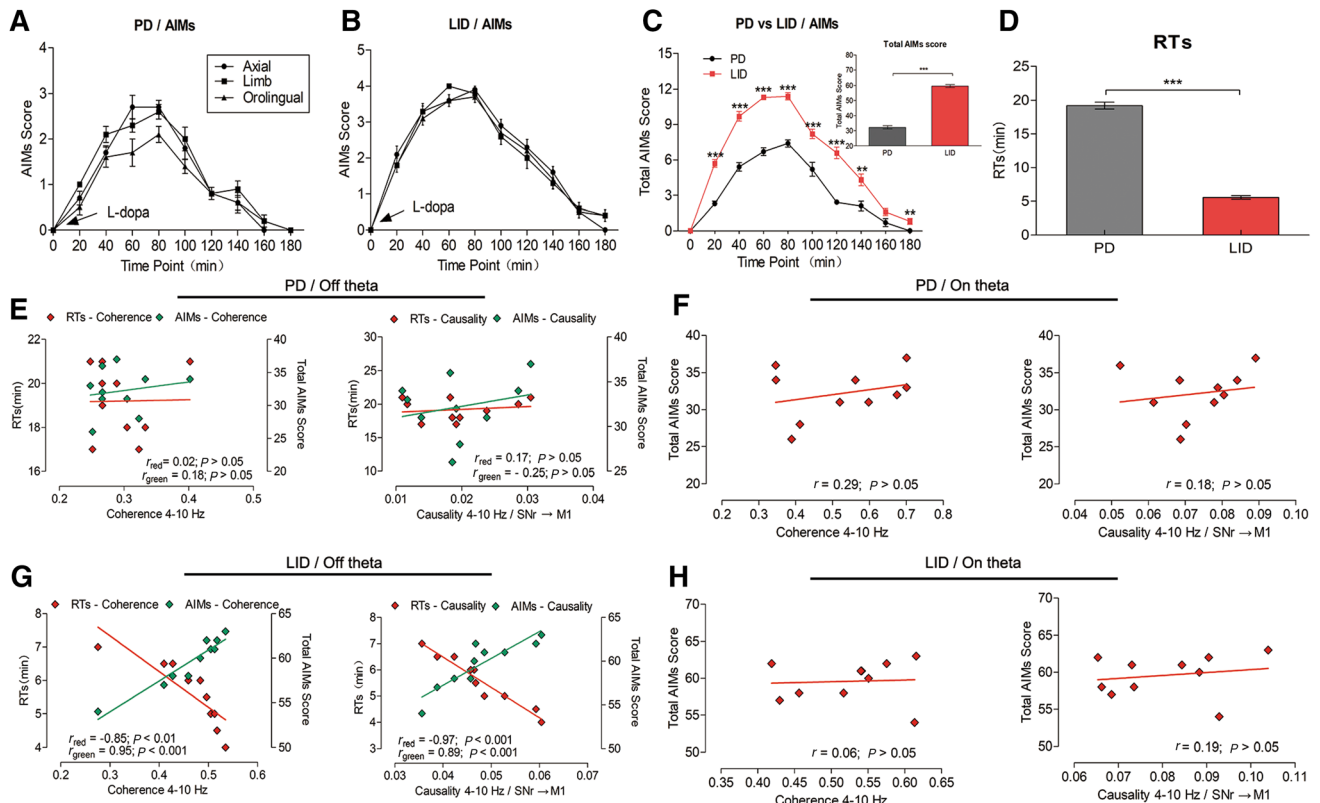


Fig. 4 Pearson correlations, represented by r values, between AIM behavior on day 0 and coherence/causality for the PD (A) and LID (B) groups. C, D Comparison of PD and LID groups' AIMs (0 min–180 min) in the on L-dopa state. Differences in AIM scores (expressed as mean \pm SEM) analyzed with rmANOVA. E RT-coherence/causality (red) and AIM-coherence/causality (green) correlations in the PD group during the off L-dopa state. F AIM-

coherence/causality correlations the PD group during the on L-dopa state. G RT(red)-coherence/causality and AIM (green)-coherence/causality correlations in the LID group during the off L-dopa state. H AIM-coherence/causality correlations in the LID group during the on L-dopa state. Correlation intensity: > 0.8 very strong; $0.6-0.8$ strong, $0.4-0.6$ moderate, $0.2-0.4$ weak, $0.0-0.2$ very weak/no correlation; $*P < 0.05$, $**P < 0.01$, $***P < 0.001$.

Pearson correlation analyses showed that, during the off L-dopa state, neither θ coherence (Fig. 4E) nor SNr \rightarrow M1 causality (Fig. 4E) in the PD group correlated significantly with AIM scores (AIMs-coherence: $r = 0.18$, $P = 0.612$; AIMs-causality: $r = -0.25$, $P = 0.493$) or RT values (RT-coherence: $r = 0.02$, $P = 0.964$; RT-causality: $r = 0.17$, $P = 0.636$). Meanwhile, during the off state, θ coherence (Fig. 4G) in the LID group had a robust negative correlation with AIM RT ($r = -0.85$, $P = 0.018$) and a very strong positive correlation with total AIM scores ($r = 0.95$, $P < 0.001$). Similarly, during the off state, SNr \rightarrow M1 causality (Fig. 4G) showed a very strong negative correlation with RT ($r = -0.97$, $P < 0.001$) and very strong positive correlation with total AIM scores ($r = 0.88$, $P < 0.001$).

In the on L-dopa state, θ coherence ($r = 0.29$, $P = 0.423$) and Granger causality ($r = 0.18$, $P = 0.624$) in the PD group remained not significantly correlated with total AIM scores (Fig. 4F). In the on state, LID group θ coherence (r

$= 0.06$, $P = 0.087$) and Granger causality ($r = 0.19$, $P = 0.607$) also did not correlate with total AIM scores (Fig. 4H).

Elto Application Reduces θ Oscillation Activity and L-dopa-Induced AIMs

LFP Activity

Analysis of LFPs on day 14, before acute L-dopa injection, showed that, during the off L-dopa state, chronic treatment with the serotonergic receptor agonist Elto reduced θ band power in M1 and the SNr (Student's t test, M1: LID 29.03 ± 0.57 vs. LID + Elto 26.29 ± 0.76 , $P = 0.02$. SNr: LID 28.31 ± 0.504 vs. LID + Elto 25.86 ± 0.83 , $P = 0.036$; Fig. 5A, B). Further coherence analysis showed a significant decrease in θ coherence in the LID+Elto group compared with the LID group (Student's t test, LID: 0.43 ± 0.07 vs. LID + Elto 0.24 ± 0.04 , $P = 0.049$, Fig. 5C).

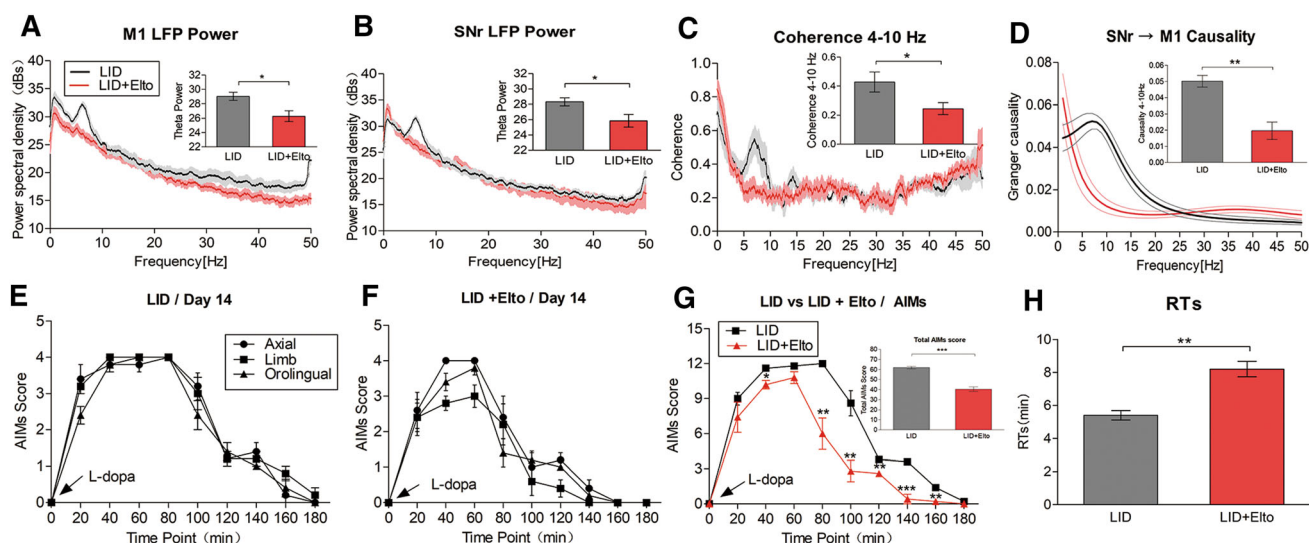


Fig. 5 Effects of Elto on θ activity in the off L-dopa state and AIMs on day 14. **A–D** Summaries of θ activity (M1 and SNr PSDs, M1–SNr coherence, Granger causality) during the off L-dopa state in LID and LID+Elto groups; bar graphs present statistical comparisons of extracted θ band data. **E, F** AIM subtype scores after L-dopa priming

(0 min–180 min) in LID and LID+Elto groups. **G** Comparison of total AIM scores from animals in panels E and F (with rmANOVA) showing Elto suppression of AIMs. **H** Comparison of AIM RT values between LID and LID+Elto groups. All data are means \pm SEMs, * P < 0.05, ** P < 0.01, *** P < 0.001.

Moreover, θ causality in the SNr \rightarrow M1 direction was decreased in the LID+Elto group compared with the LID group (Student's t test, LID: 0.05 ± 0.004 vs. LID + Elto 0.02 ± 0.005 , $P = 0.036$, Fig. 5D).

RTs and AIM Scores

Elto-induced reductions in θ activity were accompanied by strong AIM decreases. Chronic Elto reduced total AIM scores in LID rats (Student's t test, LID: 62 ± 1.14 vs. LID+Elto 40.4 ± 2.293 , $P < 0.001$, Fig. 5G). AIM scores were lower in the LID+Elto group than in the LID group in the 40th, 80th, 100th, 120th, 140th, and 160th minute observation periods (rmANOVA plus Bonferroni's *post-hoc*, P values were: 0.014, 0.002, 0.003, 0.005, < 0.001, and 0.005, respectively; Fig. 5G). RTs were extended in the LID+Elto group compared to those in the LID group (Student's t test, LID: 5.4 ± 0.29 vs. LID+Elto 8.2 ± 0.46 , $P = 0.001$; Fig. 5H).

Elto Reduces θ oscillation and Quinpirole/SKF 38393-Induced Dyskinesia

To further explore the relationship between θ activity and dyskinesia, we analyzed θ oscillation power, coherence, and Granger causality during the off L-dopa state and recorded AIMs after DA receptor agonist challenges. Systemic administration of the D2 receptor agonist quinpirole or the D1 receptor agonist SKF 38393 induced axial,

limb, and orolingual AIMs (Fig. 6G, K) that were similar to L-dopa-induced AIMs (Fig. 5E–G).

On day 16 (24-h washout on day 15), LFP recording before the quinpirole challenge showed that Elto reduced M1 and SNr θ band power in LID animals (Student's t test, M1: LID 29.94 ± 0.59 vs. LID+Elto 26.98 ± 0.43 , $P = 0.004$. SNr: LID 29.04 ± 0.77 vs. LID+Elto 25.42 ± 0.56 , $P = 0.005$; Fig. 6A, B). There was also a marked reduction in θ coherence in the LID+Elto group (0.23 ± 0.26) compared with the LID group (0.47 ± 0.37) (Student's t test, $P = 0.001$; Fig. 6C). The Elto treatment also reduced SNr \rightarrow M1 θ causality (Student's t test, LID: 0.05 ± 0.004 vs. LID+Elto 0.03 ± 0.006 , $P = 0.006$; Fig. 6D). After a single quinpirole injection, the total AIMs score in the LID+Elto group (28.2 ± 1.99) was significantly lower (Student's t test, $P < 0.001$) than that in the LID group (47.4 ± 1.86). The mean total AIM score for the LID+Elto group was significantly lower than that for the LID group 60 min, 80 min, 100 min, 120 min, and 140 min after quinpirole injection (rmANOVA: interaction: $F_{8,64} = 6.234$, $P < 0.001$; group: $F_{(1,8)} = 49.816$, $P < 0.001$; Bonferroni's *post-hoc*, $P = 0.002$, < 0.001, 0.041, < 0.001, 0.001, 0.001, Fig. 6G). Importantly, compared to the LID group (3.9 ± 0.33 s), the LID+Elto group (7.7 ± 0.37 s) exhibited a longer RT to quinpirole (Student's t test, $P = 0.001$, Fig. 6H).

On day 18 (24-h washout period on day 17), LFP recording before the SKF 38393 challenge showed that Elto reduced M1 and SNr θ band power in LID animals (Student's t test, M1: LID 29.67 ± 0.55 vs. LID + Elto 27.47 ± 0.72 , $P = 0.042$. SNr: LID 29.51 ± 0.54 vs. LID +

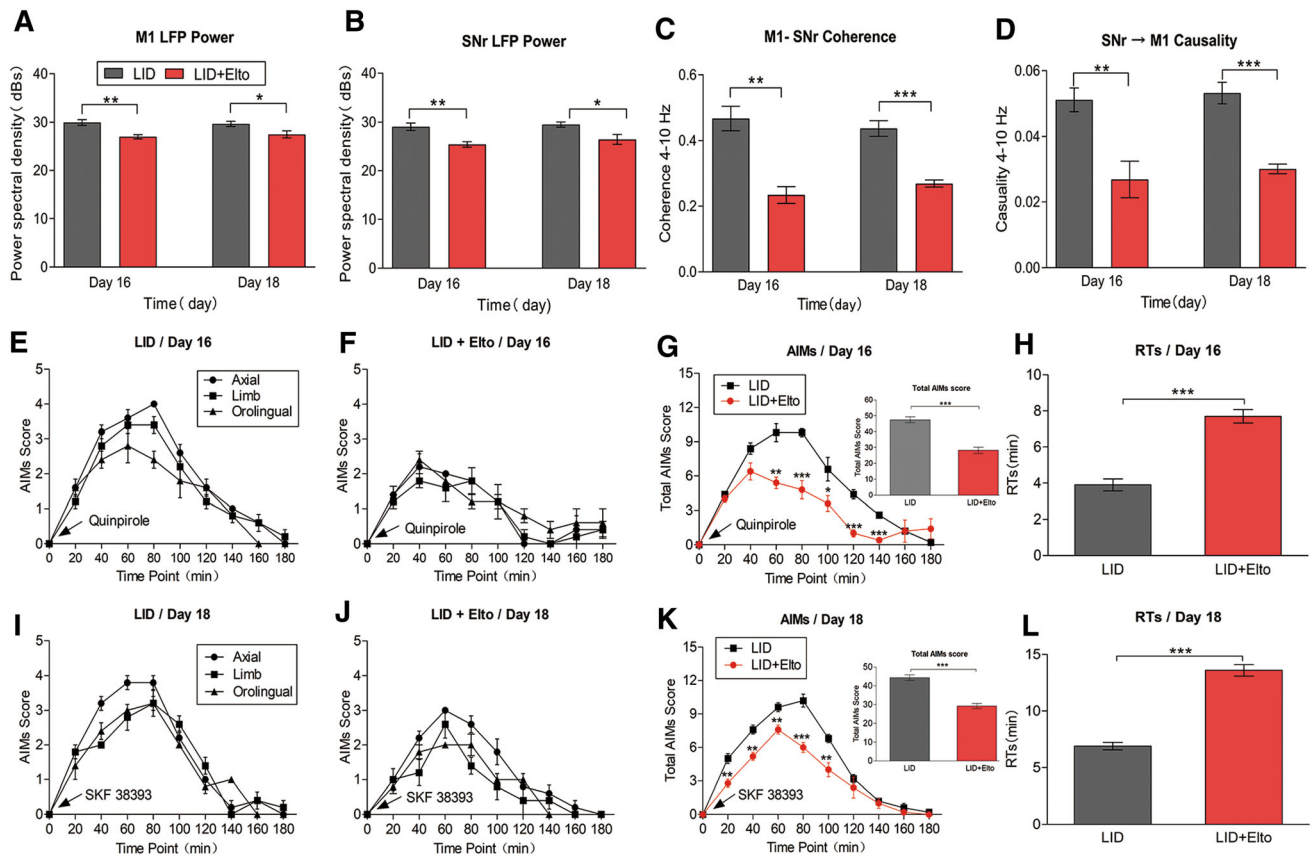


Fig. 6 DA receptor agonist induction of dyskinesia and influence on θ activity on experimental days 16 and 18. **A–D** Comparison of θ activity (PSDs, coherence, Granger causality) between and within groups. **E, F** Presence of axial, limb, and orolingual AIMs, on day 16, 0 min–180 min (20 min/session) after a single injection of quinpirole (0.2 mg/kg). **G** Comparison of AIM scores over time in the recording session (rmANOVA) on day 16 after quinpirole priming; inset graph shows a comparison of total AIM scores between LID and LID+Elto groups (Student's *t* test). **H** Comparison of RTs between LID and

LID+Elto groups (Student's *t* test) on day 16. **I, J** Presence of axial, limb, and orolingual AIMs, on day 18, 0 min–180 min (20 min/session) after a single injection of SKF 38393 (1.0 mg/kg). **K** Comparison of AIM scores over time in the recording session (rmANOVA) on day 18 after quinpirole priming; inset graph shows a comparison of total AIM scores between LID and LID+Elto groups (Student's *t* test). **L** Comparison of RTs between LID and LID+Elto groups (Student's *t* test) on day 18. All data are means \pm SEMs; * P < 0.05, ** P < 0.01, *** P < 0.001.

Elto 26.46 ± 1.01 , $P = 0.028$; Fig. 6A, B). In addition, Elto reduced θ coherence (Student's *t* test, LID: 0.44 ± 0.24 vs. LID+Elto 0.26 ± 0.11 , $P < 0.001$; Fig. 6C) and SNr→M1 θ causality (Student's *t* test, LID: 0.05 ± 0.003 vs. LID+Elto 0.03 ± 0.001 , $P = 0.001$; Fig. 6D) in LID animals. Subsequently, a single SKF 38393 injection reduced the total AIMs scores (Student's *t* test, LID: 44.4 ± 1.5 vs. LID + Elto 29.2 ± 1.36 , $P < 0.001$, Fig. 6K). The AIMs of the LID+Elto group were significantly lower than those of LID group at 20 min, 40 min, 60 min, 80 min, and 100 min after SKF 38393 injection (rmANOVA, group $F_{1,8} = 56.351$, $P < 0.001$ and interaction $F_{8,64} = 4.989$, $P < 0.001$; Bonferroni's *post-hoc*, $P = 0.005$, 0.002, 0.008, < 0.001, and 0.005, respectively; Fig. 6K). Compared with the LID group, the LID+Elto group had a longer RT to SKF 38393 (Student's *t* test, LID: 6.9 ± 0.33 vs. LID+Elto 13.6 ± 0.51 , $P < 0.001$, Fig. 6L).

Discussion

To the best of our knowledge, this study is the first to investigate the effects of chronic L-dopa on LFPs at the level of cortex-BG circuitry. We obtained three main findings: First, chronic L-dopa increased θ -band oscillation power in M1 and the SNr synchronously in LID animals. Second, θ synchronization was formed in the M1-SNr circuitry and the causal information flow was from the SNr to M1. Third, θ oscillational activity correlated strongly with the induction and development of dyskinesia. Similar to previous research, systemic administration of the D2 receptor agonist quinpirole [22, 47] and the D1 receptor agonist SKF 38393 [36, 48] independently induced axial, limb, and orolingual AIMs that were similar to L-dopa-induced AIMs.

Chronic L-dopa Priming Changes Oscillatory Activity in Off L-dopa State LID

Our study showed that enhanced θ oscillation formed in the M1 of off-state LID rats, but not in PD rats. Our results showing that chronic daily administration (21 days) of L-dopa (6 mg/kg, i.p.) plus benserazide hydrochloride (12 mg/kg, i.p.) increased the resting-state θ power in M1 expands previous local LFP recording findings showing θ band oscillation downstream of the dStr in LID rats [15]. The present findings of low-frequency oscillation also fits well with clinical findings in elderly PD patients with dyskinesia [7, 13]. In Alam's study [15], enhanced θ oscillation in off LID was considered to be the result of striatal synaptic plasticity subsequent to chronic L-dopa administration. In addition, another report in anesthetized 6-OHDA-lesioned rats also found that prolonged L-dopa treatment (21 days) contributed to adaptive electrophysiological changes (increased firing rate) in the SNr during the off LID state and the development of LID [37]. Combined with current findings, we have considerable evidence to support the speculation that L-dopa-related damage gradually alters the pathophysiological environment in the cortex and BG over time. However, the origin of θ oscillation in the BG was unclear. In the BG, θ oscillation has been attributed to specific firing patterns and has been shown to originate from particular neurons [7, 13]. Using single-neuron recording in the SNr of urethane-anesthetized LID rats, Meissner [49] found that the discharges correlated with θ oscillation in LID. Although that study did not provide direct evidence of θ oscillation in the off dyskinetic state, the findings are consistent with the supposition that θ oscillation in the off L-dopa LID state may be based on a group of single neurons with a specific firing pattern. Furthermore, θ oscillation tends to be transmitted from the dStr to the SNr [15], and we have shown previously that increased θ oscillation flowing from the dStr to SNr in the on L-dopa state LID rats correspond to signal transduction in the D1-direct pathway [35].

Our LFP recordings 60 min after a single L-dopa priming treatment (on state) linked θ oscillation closely to the presence of L-dopa. However, even though the LID group showed more AIMs than the PD group, the two groups exhibited similar θ band power levels. This disassociation between θ power and AIM scores suggests that on-state θ oscillation is unlikely to be directly related to AIM deterioration. Meissner's findings [49] suggest that on-state θ oscillation is closely related to DA metabolite concentration rather than AIM severity.

Moreover, we also found that the high β oscillation (20 Hz–38 Hz) was significantly augmented in M1 rather than the SNr in inattentive PD rats, according strongly with

several previous studies [23, 24, 43]. The absence of high β coherence and information flow during rest in PD models also indicated the importance of behavioral state when exploring mechanisms underlying the effect of DA denervation on synchronized activity in the BG and M1 [24, 50]. Interestingly, our findings on high β power showed a dramatic reduction in off LID *versus* off PD. These results are consistent with the previous finding that a progressive reduction of β oscillation emerged after prolonged L-dopa treatment for 4 weeks [23]. The opposing performance of β and θ oscillations in M1 further support an important role of β activity in the pathophysiology of LID [23].

Altered θ Functional Connectivity in Off L-dopa State LID Rats

We found that M1-SNr θ coherence was enhanced in the off-state LID group compared to the PD group, with the oscillation in M1 originating in the SNr. In PD, prior demonstrations of synchronous high β oscillation activity in M1 and the SNr [24] as well as between the STN and cortex in PD patients [51, 52] support the supposition of mutual regulation between the cortex and BG in PD [53], and further suggest that synchronous activity may occur in a BG-cortical loop in LID. Indeed, in off L-dopa LID rats, Jin [54] reported a trend of increasing θ coherence (compared with PD controls) and a significant increase in the θ phase-locked ratio between an entopeduncular nucleus spike and electrocorticography. Our coherence analyses showed strong θ synchronization between these two regions. Moreover, our Granger causality results showed that the SNr had an enhanced predictive effect on M1 oscillatory activity. The SNr has GABAergic projections to the Thal, which has glutamatergic projections to M1, forming a BG-Thal-neocortex pathway, which is well suited to be the potential neuroanatomical basis of oscillational synchronization and information flow between the SNr and M1.

The SNr, which is the main output nucleus of the BG, receives direct glutamatergic projections from the STN and direct GABAergic projections from the GPe and dStr [55]. It has been estimated that 70% of synaptic terminals in the SNr are from striatal spiny projection neurons and 15% are from the GPe [56]. Therefore, oscillatory activity in the SNr indirectly reflects the synchronous activity of the BG network [25, 57]. Bosch-Bouju *et al.* reported that BG output signals transmitted to the cortex *via* the Thal mediate BG regulation of the cortex [58]. Accordingly, the θ information flow from SNr to M1 in this study may reflect the mediation of BG synchronization on cortex.

Correlation Between Dyskinesia and θ Connectivity

Our results showed that θ coherence and SNr→M1 information flow in the off L-dopa LID state correlated negatively with RTs, and suggested that θ activity in this state is involved in the responsiveness of LID rats to an L-dopa challenge. Conversely, there was no similar RT-coherence or RT-causality correlation in PD rats. Consistent with our findings, Wang [35] showed that repeated L-dopa exposure reduces the reaction threshold of dyskinesia. Moreover, we found that θ synchronization and information flow correlated positively with AIM scores in LID rats, but not PD rats. Chronic L-dopa priming was associated with high AIM scores and a short RT in LID rats. This result is complemented by previous studies showing enhanced sensitivity to L-dopa in the SNr [59–61] or in the D1-direct pathway [9] after chronic L-dopa administration.

Our correlation analyses suggested that the intensity of θ synchronization and information flow during the on L-dopa dyskinesia state were not related to AIM severity or RTs. Although an enhanced θ oscillation normally appears after L-dopa administration in PD patients [7, 12, 13], a direct correlation between θ band power in the on L-dopa state and dyskinesia severity has not been demonstrated. Our Pearson correlation analysis support a disassociation of θ oscillations from the severity of dyskinesia. Indeed, θ oscillation was also recorded in the SNr of anesthetized LID rats without dyskinesia [49]. Likewise, abnormal θ oscillation (mean frequency at 7.38 Hz) in the STN detected in patients with diphasic dyskinesias through a deep brain stimulation electrode showed no association with dyskinesia in the presence of L-dopa [11]. What is particularly surprising about our results is the finding that θ activity correlated strongly with AIMs in the off L-dopa state, as opposed to the on L-dopa state. This finding suggests that resting-state θ functional connectivity in LID may play an important role in maintaining sensitivity to L-dopa.

We found that chronic Elto administration (13 days) reduced AIMs and increased RTs in LID rats, and these changes were accompanied by a reduction in θ oscillation activity. Our behavioral results affirmed findings [9] indicating that Elto can be used to reduce sensitivity to L-dopa, as evidenced by less severe AIMs and a more extended RT to AIM induction. With respect to mechanism, Ghiglieri *et al.* found that alleviation of dyskinesia with Elto (0.3 mg/kg, 21 days) was associated with a normalization of cAMP/PKA and ERK/mTORC signaling in the D1-direct pathway. Hence, the Elto-induced alleviation of AIMs and accompanying θ activity changes shown in the present study support the notion that θ functional

connectivity in the SNr-M1 circuit is strongly associated with AIMs in LID.

We used dyskinesia-inducing DA receptor agonist drugs to examine the relationship between θ activity associated with off L-dopa and dyskinesia. We found that systemic administration of the D2 agonist quinpirole or the D1 agonist SKF 38393 elicited AIMs in LID rats, similar to previous reports [22, 36]. Notably, a quinpirole challenge resulted in extended RTs and decreased AIM scores when given on day 16 to LID + Elto group rats that had a reduced θ band power, synchronization, and information flow relative to LID rats. Similarly, after receiving SKF 38393 on day 18, the LID + Elto group showed extended RTs and decreased AIMs, accompanied by lower θ band activity during the off L-dopa state. These results indicate that θ functional connectivity in the M1-SNr circuit is strongly correlated with the AIM behavior induced by quinpirole or SKF 38393 as well as that induced by chronic L-dopa administration. The SNr-M1 pathway was the common pathway for dyskinesia expression regardless of the type of DA receptor activated. This consistency could be related to indiscriminate transmission of θ information in the regulation of dyskinesia induced by dopaminergic activation.

It is of interest to note that the off θ oscillation in our experiment may be evoked by external sensory feedback from the repeated induction of dyskinesia. As described by Rozengurt *et al.*, θ rhythm neurofeedback benefits the early consolidation of motor sequence learning [62]. Further studies are needed to determine whether the θ activity is actively generated in the BG or is the result of external involuntary movement. In either case, we have provided direct evidence to indicate that θ oscillation in off LID originates from the cumulative effect of repeated L-dopa use and is strongly associated with dyskinesia. Moreover, θ activity is not unique to PD patients receiving L-dopa for long periods of time as it has also been recorded in parkinsonian patients with tremor [63–65], essential tremor [66], and has been defined as “tremor frequency” [65]. In addition, θ band activity has been recorded in dystonia (GPI, 4 Hz–12 Hz) [67] and Tourette’s syndrome (GPI and Thal, 3 Hz–12 Hz) [68]. Interestingly, a clinical study showed that θ synchronization between GPI and Thal represents a hyperkinetic state and has become a hyperkinetic state marker in Tourette’s syndrome [68, 69]; This result also suggested a similar effect of θ synchronization during “off” LID in our study. It should be noted that our results facilitate re-examination of “off” θ activity in PD patients [13]. The role in the underlying pathophysiology of the off-state θ and its causal relationship with dyskinesia warrants further investigation.

Our behavioral results demonstrated strong homogeneity with peak-dose dyskinesia in patients rather than biphasic dyskinesia or off-period dystonia, manifesting as chronic

L-dopa-induced dyskinesia and changed the AIMs scoring curve with time (peak at >60 min) after single L-dopa treatment (0 min–180 min). Indeed, rat AIMs exhibit functional similarities with the peak-dose dyskinesia in patients [70, 71]. These reports also indicated that the rat models of LID have excellent construct validity and provide valuable tools for discovering therapeutic targets and evaluating potential treatments for peak-dose dyskinesia [72]. Our findings on the correlation between dyskinesia and θ connectivity may provide a basis further clarification of the pathogenesis of peak-dose dyskinesia and exploring the preclinical of treatment.

Advantages and Limitations

The present experiments were designed to clarify how chronic L-dopa administration leads to neuroplastic alterations and, ultimately, the pathophysiological state of LID, including progressive deterioration of dyskinetic behavior and the associated neurophysiology. In addition, differing from anesthetized LID rats, we performed regular LFPs recordings on awake, inattentive resting rats to collect the signals that were highly correlated with dyskinesia. Whereas prior studies have focused mainly on neural activity during an on L-dopa period in LID, the present work was focused on θ oscillation during the off L-dopa state. We established and compared PD and LID models to probe the electrophysiological basis of the transition from a PD model to an LID model [14, 15]. We used a single L-dopa injection challenge and dyskinetic behavioral scoring to assess the correlation between θ oscillation in the context of chronic Elto use (13 days) and dyskinesia.

This study has several limitations. First, because we did not perform single-cell recording and analysis, we cannot identify a single-cell discharge that may be the basis for θ oscillations, limiting the ability to make inferences regarding the source of θ oscillations. The neural firing basis and cell-type specificity of θ oscillation may be clarified in future spike recording [22] and patch-clamp [73, 74] studies. Second, we cannot provide direct evidence for the reduction of θ activity by Elto. Thus the relationship between off L-dopa θ activity and dyskinesia remains imprecise. Advanced research technologies, such as optogenetics [75, 76], virus tracing [77, 78], and electrophysiology techniques can be used to elucidate a definitive relationship between θ activity and dyskinesia.

Conclusion

Our study shows that chronic L-dopa priming alters neurophysiology in the off L-dopa LID condition, as reflected by abnormal θ synchronization and information

flow in the SNr-M1 circuit. The present data further indicated that θ information flows from the SNr to M1 in the off L-dopa state in LID model rats, consistent with a regulatory influence of the BG on the neocortex. These findings suggest that information flow from the SNr to M1 may participate in dyskinesia-related information processing in the neocortex.

Acknowledgements This work was supported by the National Natural Science Foundation of China (81771210) and the Natural Science Foundation of Guangdong Province, China (2015A030313288).

Compliance with Ethical Standards

Conflict of interest The authors declare no conflict of interest to this study.

References

1. Hauser RA, Rascol O, Korczyn AD, Jon Stoessl A, Watts RL, Poewe W, *et al.* Ten-year follow-up of Parkinson's disease patients randomized to initial therapy with ropinirole or levodopa. *Mov Disord* 2007, 22: 2409–2417.
2. Rascol O, Brooks DJ, Korczyn AD, De Deyn PP, Clarke CE, Lang AE, *et al.* Development of dyskinesias in a 5-year trial of ropinirole and L-dopa. *Mov Disord* 2006, 21: 1844–1850.
3. Wang Q, Zhang W. Maladaptive synaptic plasticity in L-DOPA-induced dyskinesia. *Front Neural Circuits* 2016, 10: 105.
4. Cenci MA. Dopamine dysregulation of movement control in L-DOPA-induced dyskinesia. *Trends Neurosci* 2007, 30: 236–243.
5. Mela F, Marti M, Bido S, Cenci MA, Morari M. *In vivo* evidence for a differential contribution of striatal and nigral D1 and D2 receptors to L-DOPA induced dyskinesia and the accompanying surge of nigral amino acid levels. *Neurobiol Dis* 2012, 45: 573–582.
6. Fieblinger T, Sebastianutto I, Alcaccer C, Bimpisidisi Z, Maslava N, Sandberg S, *et al.* Mechanisms of dopamine D1 receptor-mediated ERK1/2 activation in the Parkinsonian striatum and their modulation by metabotropic glutamate receptor type 5. *J Neurosci* 2014, 34: 4728–4740.
7. Alonso-Frech F, Zamarbide I, Alegre M, Rodriguez-Oroz MC, Guridi J, Manrique M, *et al.* Slow oscillatory activity and levodopa-induced dyskinesias in Parkinson's disease. *Brain* 2006, 129: 1748–1757.
8. Foffani G, Ardolino G, Meda B, Egidio M, Rampini P, Caputo E, *et al.* Altered subthalamo-pallidal synchronisation in parkinsonian dyskinesias. *J Neurol Neurosurg Psychiatry* 2005, 76: 426–428.
9. Paolone G, Brugnoli A, Arcuri L, Mercatelli D, Morari M. Eltopazine prevents levodopa-induced dyskinesias by reducing striatal glutamate and direct pathway activity. *Mov Disord* 2015, 30: 1728–1738.
10. Silberstein P, Kuhn AA, Kupsch A, Trottenberg T, Krauss JK, Wöhrle JC, *et al.* Patterning of globus pallidus local field potentials differs between Parkinson's disease and dystonia. *Brain* 2003, 126: 2597–2608.
11. Alegre M, Lopez-Azcarate J, Alonso-Frech F, Rodriguez-Oroz MC, Valencia M, Guridi J, *et al.* Subthalamic activity during diphasic dyskinesias in Parkinson's disease. *Mov Disord* 2012, 27: 1178–1181.

12. Lofredi R, Neumann WJ, Bock A, Horn A, Huebl J, Siebert S, *et al.* Dopamine-dependent scaling of subthalamic gamma bursts with movement velocity in patients with Parkinson's disease. *Elife* 2018, 7:e31895.
13. Priori A, Foffani G, Pesenti A, Tamma F, Bianchi AM, Pellegrini M, *et al.* Rhythm-specific pharmacological modulation of subthalamic activity in Parkinson's disease. *Exp Neurol* 2004, 189: 369–379.
14. Alam M, Rumpel R, Jin X, von Wrangel C, Tschirner SK, Krauss JK, *et al.* Altered somatosensory cortex neuronal activity in a rat model of Parkinson's disease and levodopa-induced dyskinesias. *Exp Neurol* 2017, 294: 19–31.
15. Alam M, Capelle HH, Schwabe K, Krauss JK. Effect of deep brain stimulation on levodopa-induced dyskinesias and striatal oscillatory local field potentials in a rat model of Parkinson's disease. *Brain Stimul* 2014, 7: 13–20.
16. Borgkvist A, Lieberman OJ, Sulzer D. Synaptic plasticity may underlie L-DOPA induced dyskinesia. *Cur Opin Neurobiol* 2018, 48: 71–78.
17. Wu YR, Levy R, Ashby P, Tasker RR, Dostrovsky JO. Does stimulation of the GPI control dyskinesia by activating inhibitory axons? *Mov Disord* 2001, 16: 208–216.
18. Oyama G, Foote KD, Jacobson CE, Velez-Lago F, Go C, Limotai N, *et al.* GPI and STN deep brain stimulation can suppress dyskinesia in Parkinson's disease. *Parkinsonism Relat Disord* 2012, 18: 814–818.
19. Angeli A, Akram H, Zacharia A, Limousin P, Hariz M, Zrinzo L, *et al.* Varying time-course of effects of high frequency stimulation of sub-regions of the globus pallidus in patients with parkinson's disease. *Parkinsonism Relat Disord* 2015, 21: 597–602.
20. Halje P, Tamte M, Richter U, Mohammed M, Cenci MA, Petersson P. Levodopa-induced dyskinesia is strongly associated with resonant cortical oscillations. *J Neurosci* 2012, 32: 16541–16551.
21. Belic JJ, Halje P, Richter U, Petersson P, Hellgren Kotaleski J. Untangling Cortico-striatal connectivity and cross-frequency coupling in L-DOPA-induced dyskinesia. *Front Syst Neurosci* 2016, 10: 26.
22. Dupre KB, Cruz AV, McCoy AJ, Delaville C, Gerber CM, Eyring KW, *et al.* Effects of L-dopa priming on cortical high beta and high gamma oscillatory activity in a rodent model of Parkinson's disease. *Neurobiol Dis* 2016, 86: 1–15.
23. Salvade A, D'Angelo V, Di Giovanni G, Tinkhauser G, Sancesario G, Stadler C, *et al.* Distinct roles of cortical and pallidal beta and gamma frequencies in hemiparkinsonian and dyskinetic rats. *Exp Neurol* 2016, 275 Pt 1: 199–208.
24. Brazhnik E, Cruz AV, Avila I, Wahba MI, Novikov N, Ilieva NM, *et al.* State-dependent spike and local field synchronization between motor cortex and substantia nigra in hemiparkinsonian rats. *J Neurosci* 2012, 32: 7869–7880.
25. Bergman H, Feingold A, Nini A, Raz A, Slovlin H, Abeles M, *et al.* Physiological aspects of information processing in the basal ganglia of normal and parkinsonian primates. *Trend Neurosci* 1998, 21: 32–38.
26. Carta M, Carlsson T, Kirik D, Bjorklund A. Dopamine released from 5-HT terminals is the cause of L-DOPA-induced dyskinesia in Parkinsonian rats. *Brain* 2007, 130: 1819–1833.
27. Ghiglieri V, Mineo D, Vannelli A, Cacace F, Mancini M, Pendolino V, *et al.* Modulation of serotonergic transmission by eltopazine in L-DOPA-induced dyskinesia: Behavioral, molecular, and synaptic mechanisms. *Neurobiol Dis* 2016, 86: 140–153.
28. Chase A. Parkinson disease: A role for serotonergic neurons in levodopa-induced dyskinesia. *Nat Rev Neurol* 2014, 10: 180.
29. Siderowf A, Stern M. Update on Parkinson disease. *Ann Intern Med* 2003, 138: 651–658.
30. Arai R, Karasawa N, Nagatsu I. Aromatic L-amino acid decarboxylase is present in serotonergic fibers of the striatum of the rat. A double-labeling immunofluorescence study. *Brain Res* 1996, 706: 177–179.
31. Carta M, Tronci E. Serotonin system implication in L-DOPA-induced dyskinesia: From animal models to clinical investigations. *Front Neurol* 2014, 5: 78.
32. Bezdard E, Tronci E, Pioli EY, Li Q, Porras G, Bjorklund A, *et al.* Study of the antidyskinetic effect of eltopazine in animal models of levodopa-induced dyskinesia. *Mov Disord* 2013, 28: 1088–1096.
33. Svenningsson P, Rosenblad C, Arvidsson KA, Wictorin K, Keywood C, Shankar B, *et al.* Single oral treatment with the 5-HT1A/B agonist, eltopazine, counteracts L-dopa-induced dyskinesias in Parkinson's disease: A phase I/IIA, double-blind, randomized, placebo-controlled, dose-finding study. *Mov Disord* 2015, 30: S130–S130.
34. Svenningsson P, Rosenblad C, Arvidsson KA, Wictorin K, Keywood C, Shankar B, *et al.* Eltopazine counteracts L-DOPA-induced dyskinesias in Parkinson's disease: a dose-finding study. *Brain* 2015, 138: 963–973.
35. Wang Q, Chen J, Li M, Lv S, Xie Z, Li N, *et al.* Eltopazine prevents levodopa-induced dyskinesias by reducing causal interactions for theta oscillations in the dorsolateral striatum and substantia nigra pars reticulata. *Neuropharmacology* 2019, 148: 1–10.
36. Lindgren HS, Ohlin KE, Cenci MA. Differential involvement of D1 and D2 dopamine receptors in L-DOPA-induced angiogenic activity in a rat model of Parkinson's disease. *Neuropsychopharmacology* 2009, 34: 2477–2488.
37. Aristieta A, Ruiz-Ortega JA, Miguez C, Morera-Herreras T, Ugedo L. Chronic L-DOPA administration increases the firing rate but does not reverse enhanced slow frequency oscillatory activity and synchronization in substantia nigra pars reticulata neurons from 6-hydroxydopamine-lesioned rats. *Neurobiol Dis* 2016, 89: 88–100.
38. Lundblad M, Andersson M, Winkler C, Kirik D, Wierup N, Cenci MA. Pharmacological validation of behavioural measures of akinesia and dyskinesia in a rat model of Parkinson's disease. *Eur J Neurosci* 2002, 15: 120–132.
39. Winkler C, Kirik D, Bjorklund A, Cenci MA. L-DOPA-induced dyskinesia in the intrastriatal 6-hydroxydopamine model of parkinson's disease: relation to motor and cellular parameters of nigrostriatal function. *Neurobiol Dis* 2002, 10: 165–186.
40. Levesque M, Herrington R, Hamidi S, Avoli M. Interneurons spark seizure-like activity in the entorhinal cortex. *Neurobiol Dis* 2016, 87: 91–101.
41. Zhou M, Zhang W, Chang J, Wang J, Zheng W, Yang Y, *et al.* Gait analysis in three different 6-hydroxydopamine rat models of Parkinson's disease. *Neurosci Lett* 2015, 584: 184–189.
42. Bokil H, Andrews P, Kulkarni JE, Mehta S, Mitra PP. Chronux: a platform for analyzing neural signals. *J Neurosci Methods* 2010, 192: 146–151.
43. Li M, Zhou M, Wen P, Wang Q, Yang Y, Xiao H, *et al.* The network of causal interactions for beta oscillations in the pedunculopontine nucleus, primary motor cortex, and subthalamic nucleus of walking parkinsonian rats. *Exp Neurol* 2016, 282: 27–36.
44. Zhang HY, Yang J, Wang XN, Yao XM, Han HY, Gao YF, *et al.* Altered local field potential relationship between the parafascicular thalamic nucleus and dorsal striatum in hemiparkinsonian rats. *Neurosci Bull* 2019, 35: 315–324.
45. Seth AK. A MATLAB toolbox for Granger causal connectivity analysis. *J Neurosci Methods* 2010, 186: 262–273.

46. Barnett L, Seth AK. The MVGC multivariate Granger causality toolbox: a new approach to Granger-causal inference. *J Neurosci Methods* 2014, 223: 50–68.
47. Dupre KB, Eskow KL, Negron G, Bishop C. The differential effects of 5-HT1A receptor stimulation on dopamine receptor-mediated abnormal involuntary movements and rotations in the primed hemiparkinsonian rat. *Brain Res* 2007, 1158: 135–143.
48. Iderberg H, Rylander D, Bimpisidis Z, Cenci MA. Modulating mGluR5 and 5-HT1A/1B receptors to treat L-DOPA-induced dyskinesia: effects of combined treatment and possible mechanisms of action. *Exp Neurol* 2013, 250: 116–124.
49. Meissner W, Ravenscroft P, Reese R, Harnack D, Morgenstern R, Kupsch A, *et al.* Increased slow oscillatory activity in substantia nigra pars reticulata triggers abnormal involuntary movements in the 6-OHDA-lesioned rat in the presence of excessive extracellular striatal dopamine. *Neurobiol Dis* 2006, 22: 586–598.
50. Avila I, Parr-Brownlie LC, Brazhnik E, Castaneda E, Bergstrom DA, Walters JR. Beta frequency synchronization in basal ganglia output during rest and walk in a hemiparkinsonian rat. *Exp Neurol* 2010, 221: 307–319.
51. Hirschmann J, Hartmann CJ, Butz M, Hoogenboom N, Ozkurt TE, Elben S, *et al.* A direct relationship between oscillatory subthalamic nucleus-cortex coupling and rest tremor in Parkinson's disease. *Brain* 2013, 136: 3659–3670.
52. Litvak V, Jha A, Eusebio A, Oostenveld R, Foltynie T, Limousin P, *et al.* Resting oscillatory cortico-subthalamic connectivity in patients with Parkinson's disease. *Brain* 2011, 134: 359–374.
53. Oswal A, Brown P, Litvak V. Synchronized neural oscillations and the pathophysiology of Parkinson's disease. *Curr Opin Neurol* 2013, 26: 662–670.
54. Jin X, Schwabe K, Krauss JK, Alam M. Coherence of neuronal firing of the entopeduncular nucleus with motor cortex oscillatory activity in the 6-OHDA rat model of Parkinson's disease with levodopa-induced dyskinesias. *Exp Brain Res* 2016, 234: 1105–1118.
55. Nambu A. Globus pallidus internal segment. Gaba and the Basal Ganglia: From Molecules to Systems 2007, 160: 135–150.
56. Shink E, Smith Y. Differential synaptic innervation of neurons in the internal and external segments of the globus pallidus by the GABA- and glutamate-containing terminals in the squirrel monkey. *J Comp Neurol* 1995, 358: 119–141.
57. Bergman H, Wichmann T, Karmon B, DeLong MR. The primate subthalamic nucleus. II. Neuronal activity in the MPTP model of parkinsonism. *J Neurophysiol* 1994, 72: 507–520.
58. Bosch-Bouju C, Hyland BI, Parr-Brownlie LC. Motor thalamus integration of cortical, cerebellar and basal ganglia information: implications for normal and parkinsonian conditions. *Front Comput Neurosci* 2013, 7: 163.
59. Rouillard C, Bedard PJ, Falardeau P, Dipaolo T. Behavioral and biochemical evidence for a different effect of repeated administration of L-dopa and bromocriptine on denervated versus non-denervated striatal dopamine receptors. *Neuropharmacology* 1987, 26: 1601–1606.
60. Cenci MA, Lee CS, Bjorklund A. L-DOPA-induced dyskinesia in the rat is associated with striatal overexpression of prodynorphin and glutamic acid decarboxylase mRNA. *Eur J Neurosci* 1998, 10: 2694–2706.
61. Yamamoto N, Pierce RC, Soghomonian JJ. Subchronic administration of L-DOPA to adult rats with a unilateral 6-hydroxy-dopamine lesion of dopamine neurons results in a sensitization of enhanced GABA release in the substantia nigra, pars reticulata. *Brain Res* 2006, 1123: 196–200.
62. Rozenfurt R, Barnea A, Uchida S, Levy DA. Theta EEG neurofeedback benefits early consolidation of motor sequence learning. *Psychophysiology* 2016, 53: 965–973.
63. Contarino MF, Bour LJ, Bot M, van den Munckhof P, Speelman JD, Schuurman PR, *et al.* Tremor-specific neuronal oscillation pattern in dorsal subthalamic nucleus of parkinsonian patients. *Brain Stimul* 2012, 5: 305–314.
64. Tass P, Smirnov D, Karavaev A, Barnikol U, Barnikol T, Adamchic I, *et al.* The causal relationship between subcortical local field potential oscillations and Parkinsonian resting tremor. *J Neural Eng* 2010, 7.
65. Hutchison WD, Lozano AM, Tasker RR, Lang AE, Dostrovsky JO. Identification and characterization of neurons with tremor-frequency activity in human globus pallidus. *Exp Brain Res* 1997, 113: 557–563.
66. Kane A, Hutchison WD, Hodaie M, Lozano AM, Dostrovsky JO. Enhanced synchronization of thalamic theta band local field potentials in patients with essential tremor. *Exp Neurol* 2009, 217: 171–176.
67. Barow E, Neumann WJ, Brucke C, Huebl J, Horn A, Brown P, *et al.* Deep brain stimulation suppresses pallidal low frequency activity in patients with phasic dystonic movements. *Brain* 2014, 137: 3012–3024.
68. Neumann WJ, Huebl J, Brucke C, Lofredi R, Horn A, Saryyeva A, *et al.* Pallidal and thalamic neural oscillatory patterns in tourette's syndrome. *Ann Neurol* 2018, 84: 505–514.
69. Priori A, Giannicola G, Rosa M, Marceglia S, Servello D, Sassi M, *et al.* Deep brain electrophysiological recordings provide clues to the pathophysiology of Tourette syndrome. *Neurosci Biobehav Rev* 2013, 37: 1063–1068.
70. Lindgren HS, Rylander D, Ohlin KE, Lundblad M, Cenci MA. The “motor complication syndrome” in rats with 6-OHDA lesions treated chronically with L-DOPA: relation to dose and route of administration. *Behav Brain Res* 2007, 177: 150–159.
71. Dekundy A, Lundblad M, Danysz W, Cenci MA. Modulation of L-DOPA-induced abnormal involuntary movements by clinically tested compounds: further validation of the rat dyskinesia model. *Behav Brain Res* 2007, 179: 76–89.
72. Cenci MA, Crossman AR. Animal models of L-dopa-induced dyskinesia in Parkinson's disease. *Mov Disord* 2018, 33: 889–899.
73. Bateup HS, Santini E, Shen W, Birnbaum S, Valjent E, Surmeier DJ, *et al.* Distinct subclasses of medium spiny neurons differentially regulate striatal motor behaviors. *Proc Natl Acad Sci U S A* 2010, 107: 14845–14850.
74. Parker PR, Lalive AL, Kreitzer AC. Pathway-specific remodeling of thalamostriatal synapses in Parkinsonian mice. *Neuron* 2016, 89: 734–740.
75. Yizhar O, Fenno LE, Davidson TJ, Mogri M, Deisseroth K. Optogenetics in neural systems. *Neuron* 2011, 71: 9–34.
76. Gradinaru V, Mogri M, Thompson KR, Henderson JM, Deisseroth K. Optical deconstruction of parkinsonian neural circuitry. *Science* 2009, 324: 354–359.
77. Menardy F, Varani AP, Combes A, Lena C, Popa D. Functional alteration of cerebello-cerebral coupling in an experimental mouse model of Parkinson's disease. *Cereb Cortex* 2019, 29: 1752–1766.
78. Su YT, Gu MY, Chu X, Feng X, Yu YQ. Whole-brain mapping of direct inputs to and axonal projections from GABAergic neurons in the parafacial zone. *Neurosci Bull* 2018, 34: 485–496.